

# Micromachined Capacitor Ultrasonic Transducers

Butrus T. Khuri-Yakub, Mustafa Karaman, Ching-Hsiang Cheng, Sanli Ergun, Goksenin Yaralioglu, Baris Bayram, Utkan Demerci, Sean Hansen, Mohammad Badi, and Omer Oralkan

Edward L. Ginzton Laboratory  
Stanford University  
Stanford, CA 94305-4085  
USA  
FAX: 650.725.2533  
Email: [Khuri-yakub@stanford.edu](mailto:Khuri-yakub@stanford.edu)

This paper will review the use of capacitor micromachined ultrasonic transducers for the generation of longitudinal waves in gases and liquids, Lamb waves in plates, and surface waves on half spaces. Such transducers have the advantage of being fully made by surface silicon micromachining, thus enabling any type of transducer geometry by photolithography, and the possibility of electronic integration. We will present a theory that predicts the performance of the capacitor as a transducer of various modes of propagation. Next, we will present a silicon micromachining technology for making the transducers. Finally, we will present experimental results showing the performance of capacitor transducers in air (single element), water (single element, one-dimensional array, and two-dimensional arrays), and as a Lamb wave transducer on a silicon substrate. In all these applications, we will demonstrate that the capacitor transducer is a viable alternative to piezoelectric transducers. In air applications, the capacitor has a dynamic range of over 100 dBs in 100 kHz bandwidth, while in water it has over 140 dB dynamic range in 1 Hz bandwidth. For the first time, we will also show efficient excitation of A0 Lamb waves and surface waves on silicon plates.

## INTRODUCTION

Capacitors have long been used as ultrasound transducers [1]. Conventional designs have relatively large gaps, 50-100  $\mu\text{m}$ , and use the air in the gap as the restoring force of the vibrating electrode. These transducers thus suffer from low efficiency because of the relatively large gap height, and low DC electric field in the gap of the capacitor. We propose a design where silicon micromachining is used to define the capacitors. The gaps are made to be as small as 500  $\text{\AA}$ , and the restoring force of the vibrating electrode is the stiffness of the electrode itself, and electric fields in the  $10^9$  V/m are attained. This approach makes possible the fabrication of very efficient transducers. Indeed, it makes possible transducers that compete with piezoelectric transducers in terms of efficiency and bandwidth [2,3]. One advantage of these transducers is that they allow integration of electronics components on the same silicon wafer. Another is the potential for fabricating one-dimensional, two-dimensional, and annular arrays of transducers using simple photolithography. Finally, the micromachined capacitors can be used as transducers for plate modes, that is Lamb and surface waves.

## ELECTRICAL EQUIVALENT CIRCUIT MODEL OF THE TRANSDUCER

We use Mason's model to represent the capacitor transducer [4]. A schematic of the transducer and its equivalent circuit is shown in Fig. 1. A metal-coated silicon nitride membrane is used as the vibrating electrode of the capacitor. Standard integrated manufacturing processes are used to define the dimensions

of the capacitor. Residual stress in the membrane is controlled via the process of chemical vapor deposition and is held at around 100 MPas [5].

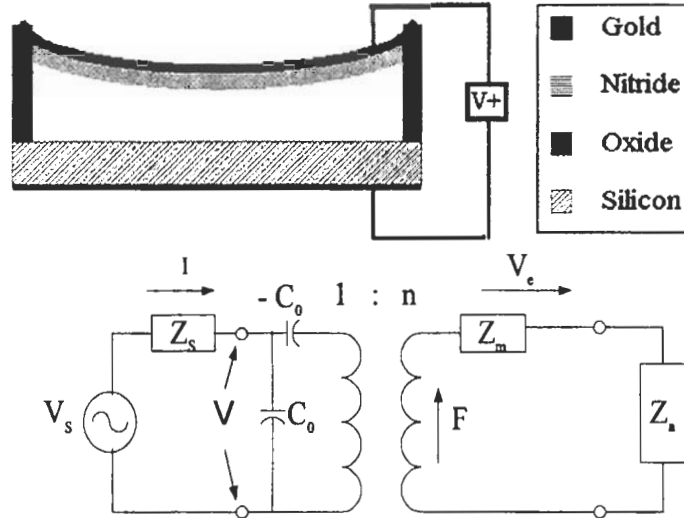


Fig. 1 Schematic diagram of a capacitor transducer and its electrical equivalent circuit.

In the equivalent circuit,  $C_0$  is the capacitance of the device,  $Z_s$  is the impedance of the source,  $Z_a$  is the impedance of the medium (air or water), and  $Z_m$  is the mechanical impedance of the circular membrane of radius 'a' which is given by:

$$Z_m = j\omega\rho l_t \left[ \frac{ak_1k_2(k_2J_0(k_1a)J_1(k_2a) + k_1J_1(k_1a)J_0(k_2a))}{ak_1k_2(k_2J_0(k_1a)J_1(k_2a) + k_1J_1(k_1a)J_0(k_2a)) - 2(k_1^2 + k_2^2)J_1(k_1a)J_1(k_2a)} \right] \quad (1)$$

where  $\omega$  is the radian frequency,  $\rho$  is the density of the membrane,  $l_t$  is the thickness of the membrane,  $J_0$  and  $J_1$  are the zeroth and first-order Bessel functions of the first kind and  $k_1$  and  $k_2$  are given by:

$$k_1 = \sqrt{\frac{\sqrt{d^2 + 4c\omega^2} - d}{2c}}, \quad k_2 = \sqrt{\frac{\sqrt{d^2 + 4c\omega^2} + d}{2c}}, \quad c = \frac{(Y_0 + T)l_t^2}{12(1 - \sigma^2)} \quad \text{and} \quad d = \frac{T}{\rho}, \quad (2)$$

where  $Y_0$  is Young's modulus,  $T$  is the residual stress and  $\sigma$  is the Poisson's ratio of the membrane material. The impedance of the membrane can be represented by a series resistance-inductance-capacitance (RLC) circuit with a resistance corresponding to the loss in the membrane.

The transformer ratio in the equivalent circuit is given by:

$$n = V_{dc} \frac{\epsilon_0 \epsilon^2 S}{(\epsilon_0 l_t + \epsilon l_a)^2}, \quad (3)$$

where  $V_{dc}$  is the dc bias on the electrode,  $\epsilon_0$  is the dielectric constant of the free space,  $\epsilon$  is the dielectric constant of the membrane material,  $S$  is the area of the transducer and  $l_a$  is the thickness of the air gap.

The importance of the approach we propose lies in the fact that the transformer ratio can be made very large. The capacitance of the capacitor can be 10 s of pFs, and the electric field can be as high as  $10^9$  V/m. This high electric field is achieved because the gap of the capacitor can be made to be as small as 500 Å. It is easy to see why the sensitivity of these capacitors is markedly higher than that of the earlier designs. The gap being several orders of magnitude smaller results in a relative change in capacitance that is the same number of orders of magnitude higher.

In a typical capacitor, each membrane is in the range of 20-100 microns in diameter. Thus, to fabricate a transducer, a very large number of membranes are electrically connected in parallel using a lithography step. This use of lithography allows the manufacture of single elements, or array elements side by side on the same wafer and in one step.

In an air transducer, the impedance of the membrane at resonance is zero and comparable in value to the impedance of air over the bandwidth. The transducer exhibits a characteristic RLC resonant behavior. Without dc bias, the real part of the input impedance is zero and the imaginary part is that of a capacitor. As the dc bias is applied, the resonant membrane introduces a real resistance resonant peak that represents real power coupled into the sound, and the imaginary part shows the characteristic acoustic "N" corresponding to potential and kinetic energy storage.

In immersion transducers the impedance of the membrane is smaller than the impedance of water and can be ignored. Thus, the input impedance of an immersion transducer has no resonance and consists only of an RC circuit in series (or parallel) [6]. Thus, impedance matching of the electronics to the RC circuit determines the bandwidth and efficiency of the transducer.

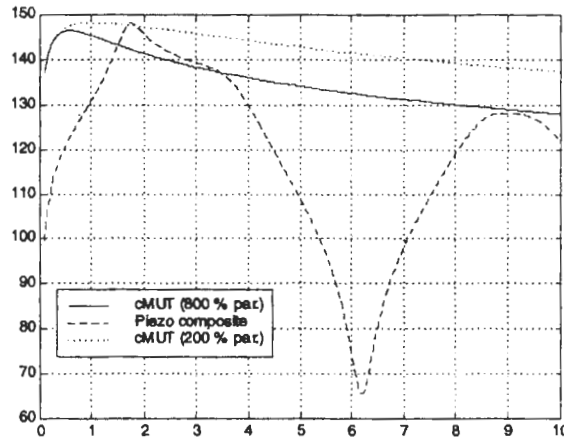


Fig. 2 Comparison of the dynamic ranges of a cMUT and a piezoelectric transducer.

The performance of a cMUT and a piezoelectric transducer are compared. For comparison, we use a square element with a side of 0.4 mm as the subject of our research program. The design calls for a center frequency of operation of 3 MHz with a bandwidth enabling operation at 0.75 MHz. The KLM model is used to represent the piezoelectric transducer, and the Mason model outlined above is used to represent the

cMUT. For the piezoelectric transducer, we use PZT 5H for the piezoelectric material and assume a perfect match into water using one matching layer. The cMUT has an air gap of 1500 Å, a silicon nitride membrane thickness of 8000 Å, a cell radius of 18 µm, and operates at a dc voltage of 100 V.

The performance of each device as a transmitter is determined by calculating the pressure at the face of the transducer that is generated by applying 1 V at its input terminals. The receiver sensitivity is calculated by evaluating the signal-to-noise level of the received voltage for an input pressure of 1 Pa at the face of the transducer. This signal-to-noise is calculated assuming an amplifier with an input resistance of 300 kΩ and capacitance of 0.3 pF. The total dynamic range of the system is calculated by adding together the transmitter and the receiver sensitivities for each transducer. Figure 2 shows the results of this comparison.

It is seen from Fig. 2 that the cMUT can have as good a dynamic range as a piezoelectric transducer over a much larger bandwidth. The minimum insertion loss and bandwidth are determined by electrical matching considerations of the transducer to the electronic circuit.

### TRANSDUCER FABRICATION

Standard integrated circuit fabrication processes are used to fabricate the cMUT. Figure 3 shows the process presently used for fabricating transducers. First, the silicon wafer receives a high-doping-density ion implantation for formation of the back contact of the capacitor. Then, a layer of insulating silicon nitride is deposited to protect the back contact and as an etch stop. An amorphous silicon sacrificial layer is deposited over the wafer. The sacrificial layer is defined by photolithography. The amorphous silicon is left in regions that are to become vacuum gaps. Another silicon nitride layer is deposited over the amorphous silicon. Holes are defined at the edges of the amorphous silicon which are then removed by wet etching. Silicon nitride is again deposited and used to plug the holes through which the etching fluid was introduced. Finally, an aluminum layer is deposited over the wafer to define the top electrode of the capacitor. An optical image of a finished device is shown in Fig. 4.



Fig. 3 Schematic of the processing schedule for fabricating cMUTs.



Fig. 4 A finished cMUT.

The individual cells are connected electrically in parallel using aluminum metal. The metal over each cell is clearly seen to be one half of the diameter of each cell. The size of the electrode is decreased to reduce the capacitance of the device without reducing the displacement at the surface of the membrane.

#### EXPERIMENTAL RESULTS

Immersion and air transducers are evaluated via measurements of their electrical input impedance, input response and bandwidth, beam profile and insertion loss. In order to fit the measured impedance of a transducer to the theoretically predicted value, a loss term has to be added to account for the insertion loss of the transducer, and a parasitic capacitance term has to be included to accurately predict the imaginary part of the impedance.

The impulse response of an immersion transducer is shown in Fig. 5. The impulse response of the transducer shows the large bandwidth that is characteristic of cMUTs. The measured fractional bandwidth is over 100%, which is limited by the electronics and not the transducer. Measurement of the insertion loss of the device shows that there is a one-way loss of 5 dB that is due to coupling into the propagation modes of the wafer.

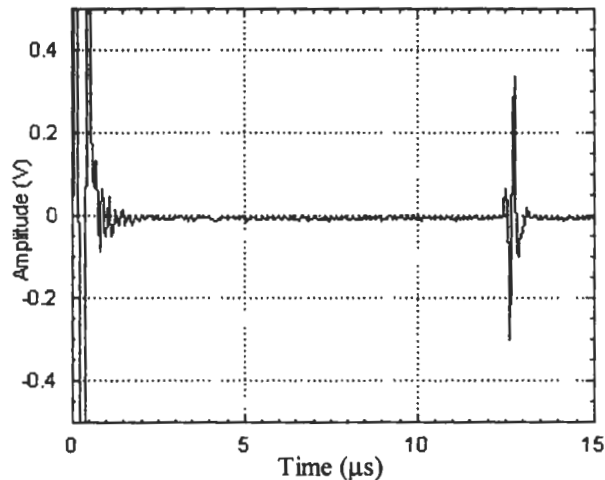


Fig. 5 Impulse response of an immersion cMUT transducer.

One of the main features of the cMUT technology is that it allows the use of photolithography to define one-dimensional or two-dimensional arrays. Another feature of cMUT arrays is that they have a thin profile, equal to the thickness of the silicon wafer. Thus, arrays can be made small to fit in tight spaces. Electronic circuits can be integrated on the same wafer as the transducers. Or, the transducer wafer can be flip-chip bonded to an electronics wafer without a significant increase in the profile of the array.

Figure 6 shows a 64-element 1-D array. The elements of the 1-D array are on 0.4 mm centers and are each 5.6 mm long. Each element consists of a number of cells that are connected in parallel in the same fashion as in single-element transducers.

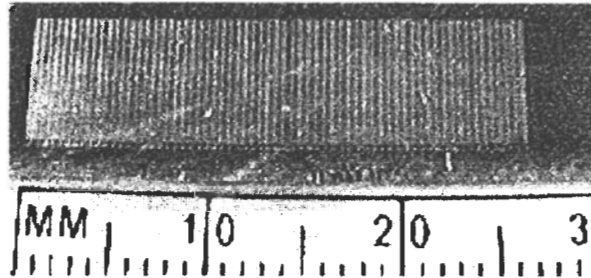


Fig. 6 A 1-D array of transducers.

The 64-element 1-D array was used to image a 0.4 mm x 0.4 mm (active area of 0.28 mm x 0.28 mm) transmitter which is placed 5 cm away in the plane perpendicular to the center of the array. The point source is excited with a pulse and all 64 elements in the array are used to receive the signal from the transmitter. Each received signal has a time delay associated with the distance between the transmitter and receiver. Typical medical imaging reconstruction algorithms are used to image a six-wires phantom as shown in Fig. 7.



Fig. 7 Reconstructed image of a six-wires phantom at 30 dB signal-to-noise ratio.

The elements of the 1-D array excite Lamb waves in the silicon wafer. This energy leaks back into the fluid and introduces ripples in the beam profile of an array element. Another source of cross talk between elements is the interface wave that propagates at the silicon water interface. These sources of cross talk and ripple in the impulse response of the transducer and its beam profile are subject of ongoing research.

Two-dimensional arrays can also be made using the same process as described above. However, there needs to be some means to connect each individual element. One method for establishing electrical connection to each element in the 2-D array is with filled through-wafer vias as shown in Fig. 8. Again, each element of the 2-D array is constructed by connecting in parallel a number of individual cells.

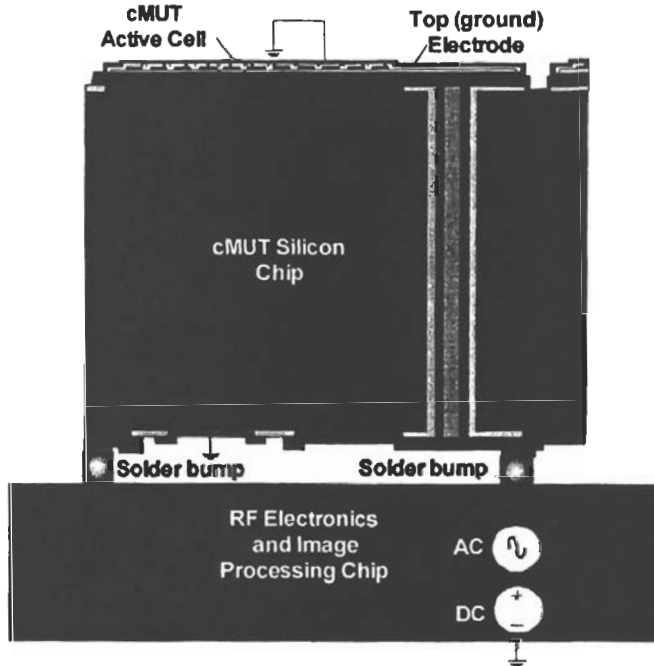


Fig. 8 Schematic diagram of a 2-D array element with a through-wafer via.

The measured acceptance angle of a 2D array element is in excellent agreement with theoretical predictions, as shown in Fig. 9. There is a slight ripple in the acceptance angle at 12° and 22° where the lowest-order antisymmetric and symmetric Lamb waves are excited at 4 MHz in a 0.5-mm-thick silicon wafer.

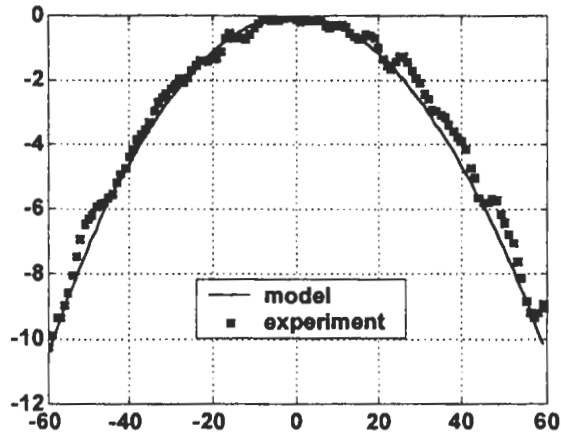


Fig. 9 Beam profile of a 0.4 mm x 0.4 mm element of a 2-D array at a frequency of 3 MHz.

The dynamic range of a 2-D element in the array is measured using a calibrated hydrophone (Specialty Engineering Associates model # PZT-Z44-0400). The output pressure at the face of the transducer, for an input voltage of 1 V, is about 20 kPa with a flat frequency response from 1 MHz to 10 MHz over the range of calibration of the hydrophone. The receiver signal-to-noise ratio is 45 dB/Pa/Hz. As seen from Fig. 10, the total dynamic range is then found to be about 130 dB/Volt/Hz. This dynamic range can be further increased by 10 dB using an amplifier with a better noise figure and by reducing the parasitic capacitance of the device. The minimum detectable pressure was measured to be 5 mPa/ $\sqrt{\text{Hz}}$ , which corresponds to a detectable displacement of  $2.5 \times 10^{-16}$  m/ $\sqrt{\text{Hz}}$ . Again, this minimum detectable noise floor can be further reduced by using a lower noise amplifier and a transducer element with a lower parasitic capacitance. The dynamic range plot shows a ripple around 1.5 MHz, which is further evidence of the coupling into Lamb waves that can be reduced.

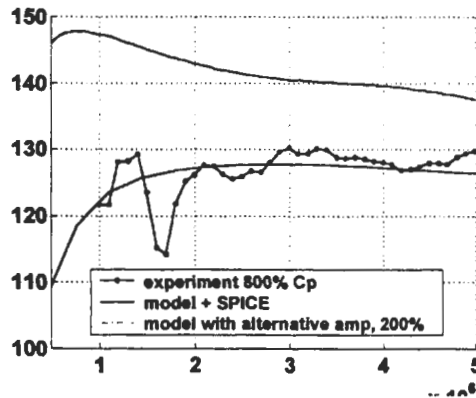


Fig. 10 Measured dynamic range of a 0.4 mm x 0.4 mm element of a 2-D array element.

As the vibrating elements are anchored into the silicon wafer, they couple energy into the substrate through their anchors. Through this means, it is possible to design transducers to couple Lamb waves and surface waves into the silicon. We calculate that at low frequencies the coupling is mostly into the lowest order Lamb waves, whereas at high frequencies, the coupling is dominated by the surface waves. Fig. 11 shows a design for a transducer for coupling the lowest order Lamb wave into the silicon wafer.

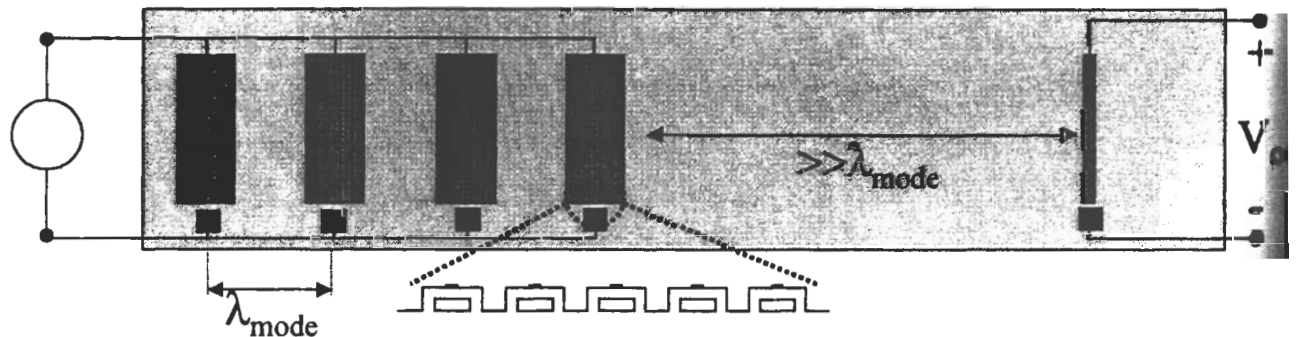


Fig. 11 Schematic diagram of a delay line using capacitor inter-digital transducer for the excitation and detection the lowest order anti-symmetric Lamb wave.

The transducer of Fig. 11 was designed to operate around 1 MHz, and the result of a through transmission experiment with this delay line is shown in Fig. 12.



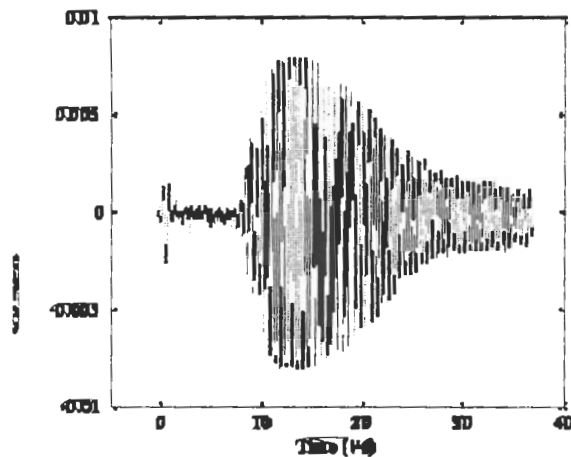


Fig. 12 Transmission through a Lamb wave delay line using capacitor interdigital transducers.

More work is needed to improve the performance of the interdigital transducers, however this experiment proves that it is possible to use cMUT structures to transmit and receive Lamb waves.

## CONCLUSIONS

Silicon micromachining can be used to fabricate capacitive ultrasonic transducers that can compete with piezoelectric transducers in terms of efficiency and bandwidth. The main reason for the promise of cMUTs is the fact that the electric field in the gap of the capacitors can be made as high as  $10^9$  V/m. Researchers in the field have recognized this fact for almost 100 years now. Only the advent of silicon micromachining has enabled this capability and brought cMUTs to the competitive edge they now demonstrate. Theory predicts the performance, and only manufacturing and characterization issues remain to be solved. Besides performance, silicon micromachining also adds the promise of ease of manufacture of one-dimensional and two-dimensional arrays and of integration with electronic circuitry.

## ACKNOWLEDGMENTS

We are grateful for the support of the Defense Advanced Research Agency, the Air Force Office of Scientific Research, and the Office of Naval Research.

## REFERENCES

1. W. Khul, G.R. Schodder, and F.K. Schodder, " *Acustica*, 4, 520 (1954).
2. M. I. Haller and B. T. Khuri-Yakub, *IEEE Trans. UFFC*, 43, 1 (1996).
3. I. Ladabaum, T. Soh, X.C. Jin, A. Atalar and B. T. Khuri-Yakub, *IEEE Trans. UFFC*, 45, 698 (1998).
4. W. P. Mason: *Electromechanical Transducers and Wave Filters*, 2<sup>nd</sup> ed (1948).
5. X. C. Jin, I. Ladabaum, and B. T. Khuri-Yakub, *IEEE/ASME J. Micro-Electro-Mechanical Syst.*, 7, 295 (1998).
6. X. C. Jin, I. Ladabaum, and B. T. Khuri-Yakub, *Proc. IEEE Workshop on Microelectromechanical Systems*, 649 (1998).
7. X. C. Jin, F. L. Degertekin, S. Calmes, X. J. Zhang, I. Ladabaum, and B.T. Khuri-Yakub, *Proc. IEEE Ultrasonic Symp.*, 1877 (1998).